Methods S1: Precipitation sampling

The sampling apparatus at Grünschwaige pasture paddock no. 8 consisted of a plastic funnel (94 mm in diameter) installed at 1 m above the soil surface and connected to a 1 L plastic collector bottle installed 1 m below ground by means of a silicone hose. A table tennis ball was placed inside the funnel to minimize evaporation losses of collected waters. The bottle was sampled and emptied regularly following rain events, i.e., at intervals of 3 to 61 days (average 14 d; n = 81).

Methods S2: MuSICA parameterisation

Parameter values for the 'standard' MuSICA runs were derived from data collected at the site (as explained in the main text and below) or taken from the literature (Table S1).

Soil

Soil structural properties (proportion of quartz and organic matter) as well as hydraulic characteristics (water retention and hydraulic conductivity) were determined on soil core samples taken at a depth of 3 to 8 cm. Soil water retention and hydraulic conductivity properties were obtained by simultaneously measuring water tension and weight changes resulting from evaporative water loss on 250 mL soil core samples, according to the simplified evaporation method (Schindler, 1980; Peters et al., 2015) using a HYPROP apparatus (UMS, Munich, Germany). Drainage and hydraulic conductivity curves were calculated from water tension and evaporative water loss data using the HYPROP software (Pertassek et al., 2015). Parameters of the van Genuchten-Mualem soil water retention model (van Genuchten, 1980; Mualem, 1976) and of the Brooks-Corey hydraulic conductivity model (Brooks and Corey, 1964), both used in MuSICA, were obtained by least-squares fit to the drainage and conductivity curves (Fig. S5). Gravitational water flow was assumed at the bottom of the mineral topsoil, at 37 cm belowground. Estimated parameter values for the soil surface resistance to water vapour transport, soil surface aerodynamic resistance and soil optical properties (albedo and emissivity) were taken from the literature (Table S1).

In the Moldrup et al. (2003) model for the water vapour effective diffusivity, the pore-size distribution parameter b was derived from the water retention curve parameters m and n as $b = 1/m/n$. In this work, we explore the consequences of using either the Penman or Moldrup soil diffusivity formulations on the prediction of the $\delta^{18}O$ signals of soil, xylem and leaf waters (see sensitivity analysis in main text).

Soil respiration (the total of root and heterotrophic soil respiration) was predicted using a Q_{10} relationship with soil surface temperature, with basal soil respiration rate at 25°C (R_{25}) and the Q_{10} value obtained from open-top chamber respiration measurements performed at the site in September 2006, May 2007 and September 2007 (Gamnitzer et al., 2009; Ostler et al., unpublished).

Notes S1: Diel measurements and modelling of ^{18}O enrichment of pasture vegetation

Leaf and soil water, and atmospheric moisture were sampled at intervals between 4 am on 4 August to 7 am on 5 August in 2005, in the centre of pasture paddock no. 8 at Grünschwaige. The procedures followed the same protocols as given in the Materials and Methods of the main text, except that soil water was collected at depths of 2, 12 and 22 cm. Leaf samples were collected every hour with three replicates, soil samples every six hours with five replicates at 2 cm, three replicates at 12 cm and one replicate at 22 cm depth.

Fig. S7 shows the diurnal cycle of observed ^{18}O enrichment of leaf water above soil water ($\Delta^{18}O_{leaf} = \delta^{18}O_{leaf} - \delta^{18}O_{soil\ 7}$), and of the $\Delta^{18}O$ predicted in the standard simulation (two-pool model with $\varphi = 0.39$) and in the Péclet simulation with $L = 167$ mm. Observed $\Delta^{18}O_{leaf}$ reached its minimum (1.9‰) at around 5 am (UTC) – pre-dawn – and then increased progressively for about 5 h to approach a near-maximum value at around 10 am. The observed $\Delta^{18}O_{leaf}$ remained within 90% of maximum for about 5 h and then decreased continuously for about 12 h to reach another minimum (at ~0.1‰) at 2 to 5 am the next morning.

These $\Delta^{18}O_{leaf}$ data were used to fine-tune the parameters controlling leaf water enrichment in MuSICA, mainly mesophyll water content, the Péclet effective length and stomatal conductance parameters such as nighttime and residual stomatal conductance, within the known range for temperate grassland or cool-season grasses. Following these adjustments, modelled $\Delta^{18}O_{leaf}$ followed quite closely the temporal pattern of observed $\Delta^{18}O_{leaf}$ when a two-pool model was applied. In particular, the maximum of modelled $\Delta^{18}O_{leaf}$ was reached at approximately the same time as that observed. By contrast, when a Péclet model with a constant mixing length was applied in the simulation, predicted $\Delta^{18}O_{leaf}$ reached a maximum in the late afternoon and evening hours that was not present in the observed data (Fig. S7).

Notes S2: Testing the relevance of the Péclet effect in the pasture species *Lolium perenne* and *Dactylis glomerata* in controlled environments

Several recent studies (Roden et al., 2015; Song et al., 2015) have called into question the relevance of the Péclet effect to leaf water isotopes. Given this uncertainty, and the added complexity of including a Péclet effect in leaf water models, we tested the requirement for a Péclet effect in the pasture grasses *L. perenne* and *D. glomerata* – two of the co-dominant species in the grassland ecosystem study – with an aim to applying Occam's razor principle if appropriate (Figs. S12-13).

Lolium perenne

Perennial ryegrass seeds (*L. perenne* L. cv. Bronsyn plus AR1 endophyte, 2 g per pot or 83 g m^{-2}) were sown into 5-L pots containing 1700 g of seed-raising mix at field capacity and grown in a controlled-environment growth cabinet maintained at 20°C, 70% RH, 700 µmol m^{-2} s^{-1} PAR during the 16-h light period, and 15°C, 70% RH during the 8-h dark period, for 17 d. The pots were then randomly allocated to either high (70%) or low (30%) relative humidity cabinets in which all other settings were the same. All plants were clipped to 6 cm in height, and well-watered daily. Seven days after the humidity

treatments were applied, eight pots within each humidity treatment were allocated to either well-watered (field capacity) or droughted (midway between field capacity and oven-dried water content) treatments. Plants in these pots were again clipped to 6 cm in height. Water content was maintained in both treatments by daily gravimetric measurements, with water used replaced. Plants were grown for 21 days after the commencement of the water treatment and droughted pots took 2-3 days to reach their target water content.

Leaf gas exchange measurements occurred between 8 and 16 days after the start of the water treatment, and leaf water sampling on day 20 of the treatment. Transpiration rate (E) was measured on a group of 10-20 leaves in each of 5 pots per treatment over a 24 hour period under growth conditions using a custom clear-top chamber fitted to a Li6400 (LiCor Inc., Lincoln, NE, USA) photosynthesis system (as described in Loucos et al., 2015, except that the incident light within the growth cabinet was used rather than an external light source). Measurements were recorded every minute, averaged over 10 minutes, then a treatment average calculated to compare to leaf samples taken from randomly-assigned pots every two hours. Every 2 hours when the cabinet lights were on during a 29 hour period, three leaves (3 cm in length) were cut and immediately placed in small glass vials, then flushed with 2% CO_2 and sealed. The oxygen in leaf water was left to equilibrate with oxygen in CO_2 within the vial for 48 hours at 25°C, then the CO_2 was analysed for $\delta^{18}O$ on a tunable diode laser absorption spectrometer (TDL, TGA100A, Campbell Scientific) as described by Song and Barbour (2016), with liquid water standards for correct isotope compositions of the leaf water relative to SMOW.

The isotope composition of water vapour and irrigation water was measured on the TDL as described above. Water vapour was collected by pumping air from each growth cabinet through a glass cold finger trap sitting in an ethanol-dry ice slurry. Air was pumped for 20 minutes for the low RH cabinet and 10-25 minutes for the high RH cabinet, and collections were made every 2 hours. The irrigation water had a $\delta^{18}O$ of -9.6‰, while the water vapour varied between -18.2 and -14.0‰ (the low RH cabinet had significantly less enriched water vapour than did the high RH; -16.0 ± 0.4‰ compared to -17.2 ± 0.3‰, $P = 0.003$). Irrigation water and vapour $\delta^{18}O$ were used to calculate $\Delta^{18}O_{e,ss}$ (using Eq. (2), main text) and measured leaf water enrichment, $\Delta^{18}O_{leaf}$.

The Péclet effect predicts a positive relationship between E and the proportional difference between $\Delta^{18}O_{leaf}$ and $\Delta^{18}O_e$, but it can be seen from Figure S12 that variation in E explained very little variation in the proportional difference, suggesting that the Péclet effect was of limited relevance for *L. perenne*.

Dactylis glomerata

We also tested the relevance of the Péclet effect on a second, small stature grass species using the online gas exchange and equilibrated leaf water method developed by Song et al. (2015). *D. glomerata* L. plants were grown from seed in 7-L pots with potting mix amended with slow release fertiliser (Osmocote, Scotts Australia Pty Ltd., Sydney, NSW, Australia) in a controlled environment room set at day/night temperature of 28/20 ºC, 75% air humidity in the day and night, 14 h day period and an approximate irradiance at the top of the canopy of 600 µmol m^{-2} s^{-1}. When the plants were 60 days old, 3-5 leaves were sealed in a 2 × 3 cm leaf chamber with a red-blue light source attached to a Li6400 photosynthesis system and

plumbed to a water vapour isotope analyser (L1102-i; Picarro Inc., Sunnyvale, CA, USA) for isotopologue measurement. Dry air entered the leaf chamber, so that all the water vapour measured by the analyser came from transpiration (*E*). The conditions inside the leaf chamber were manipulated to achieve a range in *E*, by altering flow rate through the chamber (between 250 and 700 μmol s^{-1}) and CO_2 concentration (between 100 and 500 μmol mol^{-1}), while temperature and irradiance were held constant (30°C and 2000 μmol m^{-2} s^{-1}, respectively). Leaves remained in the chamber for 15-20 minutes, after which they were rapidly sampled into glass vials, flushed with 2% CO_2 and sealed prior to equilibration and subsequent isotope analysis as described above (following Song and Barbour, 2016).

There was no significant relationship between *E* and the proportional difference in *D. glomerata* using the online transpiration technique, consistent with the observation in *L. perenne* (Fig. S13).

References

Atkin, O. K., Westbeek, M., Cambridge, M. L., Lambers, H., and Pons, T. L.: Leaf respiration in light and darkness (a comparison of slow- and fast-growing *Poa* species), Plant Physiol., 113, 961–965, https://doi.org/10.1104/pp.113.3.961, 1997.

Ball, J. T., Woodrow, I. E., and Berry, J. A.: A Model Predicting Stomatal Conductance and its Contribution to the Control of Photosynthesis Under Different Environmental Conditions, in: Progress in photosynthesis research (vol. 4), edited by: Biggins, J., Martinus Nijhoff Publishers, Dordrecht, the Netherlands, 221–224, https://doi.org/10.1007/978-94-017-0519-6_48, 1987.

Braud, I., Dantas-Antonino, A. C., Vauclin, M., Thony, J. L., and Ruelle, P.: A simple soil-plant-atmosphere transfer model (SiSPAT) development and field verification, J. Hydrol., 166, 213–250, https://doi.org/10.1016/0022-1694(94)05085-C, 1995.

Brooks, R. H. and Corey, A. T.: Hydraulic properties of porous media, Hydrology Paper no. 3, Civil Engineering Dep., Colorado State Univ., Fort Collins, Colo, 1964.

Collatz, G. J., Ball, J. T., Grivet, C., and Berry, J. A.: Physiological and environmental regulation of stomatal conductance, photosynthesis and transpiration: a model that includes a laminar boundary layer, Agr. Forest Meteorol., 54, 107–136, https://doi.org/10.1016/0168-1923(91)90002-8, 1991.

Deardorff, J. W.: Efficient prediction of ground surface temperature and moisture, with inclusion of a layer of vegetation, J. Geophys. Res., 83, 1889–1903, https://doi.org/10.1029/JC083iC04p01889, 1978.

Farquhar, G. D. and Wong, S. C.: An empirical model of stomatal conductance, Funct. Plant Biol., 11, 191–210, https://doi.org/10.1071/PP9840191, 1984.

Farquhar, G. D., von Caemmerer, S., and Berry, J. A.: A biochemical model of photosynthetic CO_2 assimilation in leaves of C_3 species, Planta, 149, 78–90, https://doi.org/10.1007/BF00386231, 1980.

Gamnitzer, U., Schäufele, R., and Schnyder, H.: Observing ^{13}C labelling kinetics in CO_2 respired by a temperate grassland ecosystem, *New Phytol.,* **184,** 376–386, https://doi.org/10.1111/j.1469-8137.2009.02963.x, 2009.

van Genuchten, M. T. H.: A closed-form equation for predicting the hydraulic conductivity of unsaturated soils, *Soil Sci. Soc. Am. J.,* **44**, 892–898, https://doi.org/10.2136/sssaj1980.03615995004400050002x, 1980.

Harley, P. C., Thomas, R. B., Reynolds, J. F., and Strain, B. R.: Modelling photosynthesis of cotton grown in elevated CO_2, *Plant Cell Environ.,* **15**, 271-282, https://doi.org/10.1111/j.1365-3040.1992.tb00974.x, 1992.

Jackson, R. D.: Surface temperature and the surface energy balance, in: Flow and Transport in the Natural Environment: Advances and Applications, edited by: Steffen, W. L. and Denmead, O. J., Springer, Berlin, Heidelberg, 133-153, https://doi.org/10.1007/978-3-642-73845-6_9, 1988.

Kelliher, F. M., Black, T. A., and Price, D. T.: Estimating the effects of understory removal from a douglas fir forest using a two-layer canopy evapotranspiration model, Water Resour. Res., 22, 1891-1899, https://doi.org/10.1029/WR022i013p01891, 1986.

Loucos, K. E., Simonin, K. A., Song, X., and Barbour, M. M.: Observed relationships between leaf $H_2{}^{18}O$ Péclet effective length and leaf hydraulic conductance reflect assumptions in Craig-Gordon model calculations, Tree Physiol., 35, 16–26, https://doi.org/10.1093/treephys/tpu110 , 2015.

Massman, W. J. and Weil, J. C.: An analytical one-dimensional second-order closure model of turbulence statistics and the Lagrangian time scale within and above plant canopies of arbitrary structure, Bound.-Lay. Meteorol., 91, 81–107, https://doi.org/10.1023/A:1001810204560, 1999.

Medlyn, B. E., Dreyer, E., Ellsworth, D., Forstreuter, M., Harley, P. C., Kirschbaum, M. U. F., Le Roux, X., Montpied, P., Strassemeyer, J., Walcroft, A., Wang, K., and Loustau, D.: Temperature response of parameters of a biochemically based model of photosynthesis. II. A review of experimental data, Plant Cell Environ., 25, 1167–1179, https://doi.org/10.1046/j.1365-3040.2002.00891.x, 2002.

Miner, G. L., Bauerle, W. L., and Baldocchi, D. D.: Estimating the sensitivity of stomatal conductance to photosynthesis: a review, Plant Cell Environ., 40, 1214–1238, https://doi.org/10.1111/pce.12871, 2017.

Moldrup, P., Olesen, T., Komatsu, T., Yoshikawa, S., Schjønning, P., and Rolston, D. E.: Modeling diffusion and reaction in soils: X. A unifying model for solute and gas diffusivity in unsaturated soil, Soil Sci., 168, 321-337, DOI: 10.1097/01.ss.0000070907.55992.3c, 2003.

Monteith, J. L. and Unsworth, M. H.: Principles of Environmental Physics, second edition, Elsevier, Amsterdam, Netherlands, 1990.

Mualem, Y.: A new model for predicting the hydraulic conductivity of unsaturated porous media, Water Resour. Res., 12, 513–522, https://doi.org/10.1029/WR012i003p00513, 1976.

Nikolov, N., Massman, W., and Schoettle, A.: Coupling biochemical and biophysical processes at the leaf level: an equilibrium photosynthesis model for leaves of C_3 plants, Ecol. Model., 80, 205–235, https://doi.org/10.1016/0304-3800(94)00072-P, 1995.

Ogée, J. and Brunet, Y.: A forest floor model for heat and moisture including a litter layer, J. Hydrol., 255, 212–233, https://doi.org/10.1016/S0022-1694(01)00515-7, 2002.

Pertassek, T., Peters, A., and Durner, W.: HYPROP-FIT Software User's Manual, V.3.0, UMS GmbH, Munich, Germany, 2015.

Peters, A., Iden, S. C., and Durner, W.: Revisiting the simplified evaporation method: Identification of hydraulic functions considering vapor, film and corner flow, J. Hydrol., 527, 531-542, https://doi.org/10.1016/j.jhydrol.2015.05.020, 2015.

Picon-Cochard, C., Pilon, R., Tarroux, E., Pagès, L., Robertson, J., and Dawson, L.: Effect of species, root branching order and season on the root traits of 13 perennial grass species, Plant Soil, 353, 47–57, https://doi.org/10.1007/s11104-011-1007-4, 2012.

Roden, J., Kahmen, A., Buchmann, N., and Siegwolf, R.: The enigma of effective path length for ^{18}O enrichment in leaf water of conifers, Plant Cell Environ., 38, 2551–2565, https://doi.org/10.1111/pce.12568, 2015.

Rogers, A., Fischer, B. U., Bryant, J., Frehner, M., Blum, H., Raines, C. A., and Long, S. P.: Acclimation of photosynthesis to elevated CO_2 under low-nitrogen nutrition is affected by the capacity for assimilate utilization. Perennial ryegrass under free-air CO_2 enrichment, Plant Physiol., 118, 683–689, https://doi.org/10.1104/pp.118.2.683, 1998.

Schaap, M. G. and Bouten, W.: Forest floor evaporation in a dense Douglas fir stand, J. Hydrol., 193, 97-113, https://doi.org/10.1016/S0022-1694(96)03201-5, 1997.

Schindler, U.: Ein Schnellverfahren zur Messung der Wasserleitfähigkeit im teilgesättigten Boden an Stechzylinderproben, Arch. Acker Pfl. Boden., 24, 1-7, 1980.

Schleip, I.: Carbon residence time in above-ground and below-ground biomass of a grazed grassland community, Ph.D. thesis, Technical University of Munich, 2013.

Sellers, P. J.: Canopy reflectance, photosynthesis and transpiration, Int. J. Remote Sens., 6, 1335–1372, https://doi.org/10.1080/01431168508948283, 1985.

Song, X. and Barbour, M. M.: Leaf water oxygen isotope measurement by direct equilibration, New Phytol., 211, 1120-1128, https://doi.org/10.1111/nph.13962, 2016.

Song, X., Loucos, K. E., Simonin, K. A., Farquhar, G. D., and Barbour, M. M.: Measurements of transpiration isotopologues and leaf water to assess enrichment models in cotton, New Phytol., 206, 637–646, https://doi.org/10.1111/nph.13296, 2015.

Warren, C. R.: Stand aside stomata, another actor deserves centre stage: the forgotten role of the internal conductance to CO_2 transfer, J. Exp. Bot., 59, 1475–1487, https://doi.org/10.1093/jxb/erm245, 2008.

Wohlfahrt, G., Bahn, M., Horak, I., Tappeiner, U., and Cernusca, A.: A nitrogen sensitive model of leaf carbon dioxide and water vapour gas exchange: application to 13 key species from differently managed mountain grassland ecosystems, Ecological Modelling, 113, 179–199, https://doi.org/10.1016/S0304-3800(98)00143-4, 1998.

Wohlfahrt, G., Bahn, M., Newesely, C., Sapinsky, S., Tappeiner, U., and Cernusca, A.: Canopy structure versus physiology effects on net photosynthesis of mountain grasslands differing in land use, Ecol. Model., 170, 407–426, https://doi.org/10.1016/S0304-3800(03)00242-4, 2003.

Wullschleger, S. D.: Biochemical limitations to carbon assimilation in C_3 plants – a retrospective analysis of the A/C_i curves from 109 species, J. Exp. Bot., 44, 907–920, https://doi.org/10.1093/jxb/44.5.907, 1993.

Table S1: Soil and plant parameters used in the standard MuSICA simulations.

Parameter	Symbol	Value	Unit	Comment [A]
SOIL				
Structural characteristics				
Depth	d_{soil}	0.37	m	measured
Quartz fraction	f_{quartz}	0.16	% (w/w)	measured
Organic fraction	$f_{organic}$	0.07	% (w/w)	measured
Remaining soil fraction	$f_{remaining}$	0.77	% (w/w)	measured
Bulk density	D_b	1.33	g cm^3	measured
Hydraulic characteristics				
Saturated water content	θ_{sat}	0.49	m^3 m^{-3}	calculated from water retention curve
Residual water content	θ_{sat}	0.01	m^3 m^{-3}	calculated from water retention curve
Retention curve inflection point	α^{-1}	0.43	m	calculated from water retention curve
Retention curve shape factor	m_{ret}	0.13	-	calculated from water retention curve
Hydraulic conductivity at saturation	K_{sat}	0.29	m d^{-1}	calculated from hydraulic conductivity measurement
Preferential flow				
Fraction of cracks	f_{crack}	0.02	-	estimated
Depth of cracks	d_{crack}	0.1	m	estimated
Resistance to water transport through soil surface pores				
Minimum resistance	$r_{s,min}$	800	s m^{-1}	Kelliher et al. (1986)
Maximum resistance	$r_{s,max}$	16100	s m^{-1}	Kelliher et al. (1986)
Threshold water content	θ_{tr}	0.194	m^3 m^{-3}	Schaap and Bouten (1997), Ogée and Brunet (2002)
Soil and root respiration				
Respiration at 25 ^oC	R_{25}	8.5	µmol m^{-2} s^{-1}	Gamnitzer et al. (2009), Ostler et al. (unpublished)
Base for exponential soil respiration eqn.	Q_{10}	2.2	-	

Surface optical properties				
Surface albedo (of litter or mosses) for visible light	α_{vis}	0.15	-	Deardorff (1978)
Surface albedo (of litter or mosses) for near-infrared light	α_{nir}	0.60	-	--
Surface emissivity	ε_{soil}	0.95	-	Deardorff (1978)
Soil surface aerodynamic resistance				
Aerodynamic coefficient	C_u	33	-	Ogée and Brunet (2002)
VEGETATION				
Canopy structure				
Canopy height	h_{canopy}	0.078	m	estimated from sward height measurements
Leaf area index	LAI	2.6		estimated from sward height measurements
Mean relative height of vertical leaf area density profile	μ_b	0.315	-	based on Wohlfahrt et al. (2003)
Standard deviation of vertical leaf area density profile	σ_b	0.21	-	based on Wohlfahrt et al. (2003)
Leaf inclination index	LII	0	-	estimated from sward height measurements
Leaf photosynthesis				
Maximum rate of carboxylation at 25°C	V_{cmax}	60	μmol m^{-2} s^{-1}	Rogers et al. (1998)
Potential rate of electron transport at 25 °C	J_{max}	100	μmol m^{-2} s^{-1}	calculated from V_{cmax} following Medlyn et al. (2002)
Temperature optimum for V_{cmax}	$T_{opt.V}$	40	°C	Harley et al. (1992)
Temperature optimum for J_{max}	$T_{opt.J}$	35	°C	Harley et al. (1992)
Curvature of *J*-PAR relationship	θ_J	0.85	-	-
Efficiency of light energy conversion (electrons per photon)	α_J	0.18	mol mol^{-1}	Wullschleger (1993) and papers cited therein
Dark respiration rate at 25 °C	R_d	0.86	μmol m^{-2} s^{-1}	Ostler et al. (unpublished)
Light inhibition factor for R_d	I	0.5	-	cf. Atkin et al. (1997)

Stomatal conductance				
Intercept	g_o	10	mmol m^{-2} s^{-1}	Collatz et al. (1991)
Slope	m_{gs}	10	-	Miner et al. (2017), and references therein
Critical water potential	Ψ_{gs50}	-1.5	MPa	Braud et al. (1995)
Steepness parameter	v	4	-	Nikolov et al. (1995)
Minimum conductance for dawn and dusk conditions	g_{min}	10	mmol m^{-2} s^{-1}	-
Maximum nocturnal conductance	g_{night}	30	mmol m^{-2} s^{-1}	fitted (see SI text)
VPD threshold for nocturnal conductance	VPD_{thresh}	0.10	MPa	-
Mesophyll conductance				
Maximum mesophyll conductance	g_m	0.35	mol m^{-2} s^{-1}	Warren (2008)
Leaf boundary-layer conductance				
Leaf size	d	8	mm	measured and estimated (see SI text)
Shoot size	d_s	78	mm	calculated from sward height measurements
Shelter factor	P_d	1.3	-	Monteith and Unsworth, 1990
Root distribution				
Mean of the β-distribution	μ_{root}	0.105		estimated
Standard deviation of the β-distribution	σ_{root}	0.06		estimated
Mean root length density		19	km m^{-2}	estimated (see Materials and Methods)
Root hydraulics				
Fine root radius	r	0.15	mm	Picon-Cochard et al. (2012)
Root hydraulic resistance	R_{root}	1	Ts m^{-1}	estimated
Total internal storage capacity	W_{cap}	0.01	kg m^{-2} MPa^{-1}	estimated
Leaf optical properties				
Reflectance for visible light	ρ_{vis}	0.105	-	Sellers (1985)

Reflectance for near-infrared light	ρ_{nir}	0.577	-	Sellers (1985)
Transmittance for visible light	τ_{vis}	0.07	-	Sellers (1985)
Transmittance for near-infrared light	τ_{nir}	0.248	-	Sellers (1985)
Leaf emissivity	ε_{leaf}	0.98	-	Nikolov et al. (1995); Braud et al. (1995); Jackson (1988)
Rain interception				
Water storage capacity	S	0.1	mm m^{-2}	
Exponent for power function		0.67		Deardorff (1978); Braud et al. (1995)
Wind attenuation				
Canopy drag coefficient	C_d	0.2	-	Massman and Weil (1999)
Leaf water isotope modelling				
Mesophyll water content	$W_{mesophyll}$	2	mol m^{-2}	fitted (see SI text)
Proportion of unenriched leaf water	φ	0.39	-	this work
Peclet effective length	L	0.162	m	this work

[A] For details of parameter estimation or measurements, see Materials and Methods in main text and Supplemental Information

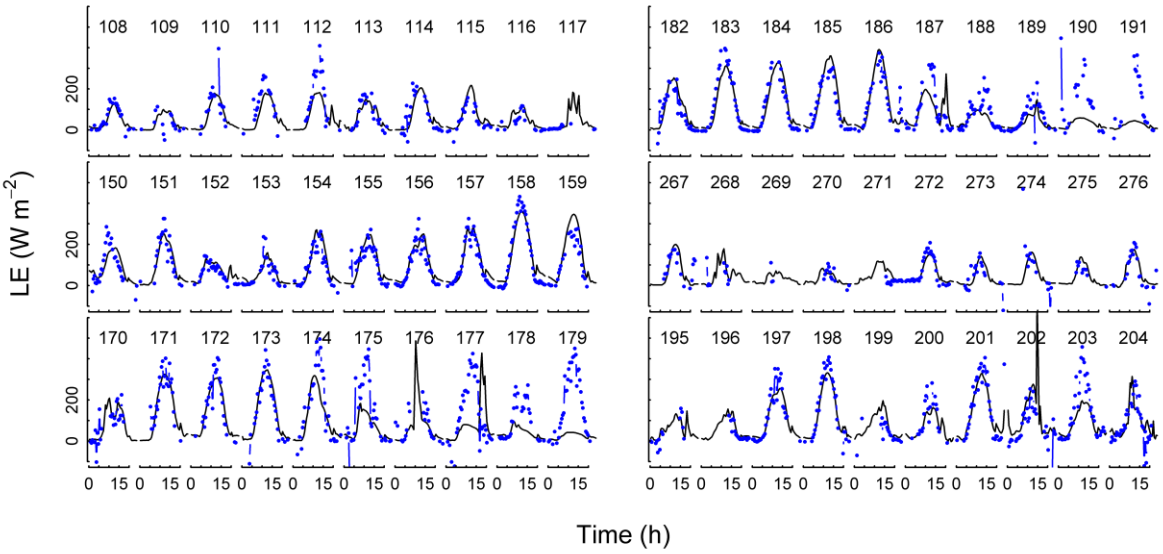

Figure S1: Comparison of latent heat flux obtained from eddy flux data (blue dots) and latent heat flux predicted by the MuSICA model in standard parameterisation (continuous black line). Panels show 10 d-long periods selected randomly from the first (left panels) and second half (right) of the vegetation periods of 2006 (top) to 2008 (bottom). The numbers above the diurnals indicate the day of the year. Time is given in UTC. Both data sets were obtained at pasture paddock no. 8 of Grünschwaige Grassland Research Station. The relationship between eddy flux- and MuSICA-based estimates of latent heat fluxes for the entire 2006-2008 data set was not biased and had an $R^2 = 0.60$.

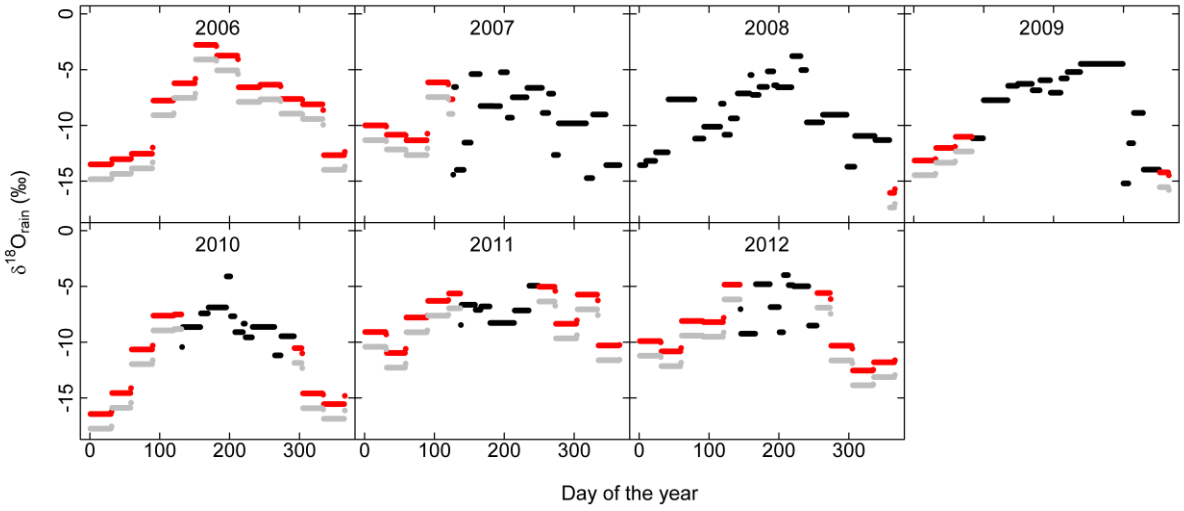

Figure S2: $\delta^{18}O$ of rain water ($\delta^{18}O_{rain}$) collected at the experimental site (black symbols), along with IsoGSM predictions (red symbols) and corrected IsoGSM predictions of $\delta^{18}O_{rain}$ (grey symbols). The latter were obtained by subtracting the mean offset (–1.3‰; cf Fig. S3) between $\delta^{18}O_{rain}$ observed at the site and IsoGSM predictions from the non-corrected IsoGSM data.

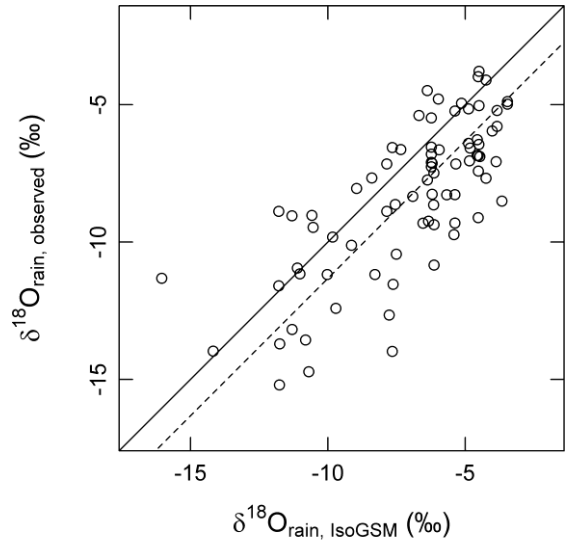

Figure S3: Relationship between the $\delta^{18}O$ of rainwater collected at the experimental site ($\delta^{18}O_{rain,\ observed}$) and the $\delta^{18}O$ of monthly IsoGSM predictions ($\delta^{18}O_{rain,\ IsoGSM}$). The solid line represents the 1:1 relation; the dashed line illustrates the mean difference between the two data sets (–1.3‰).

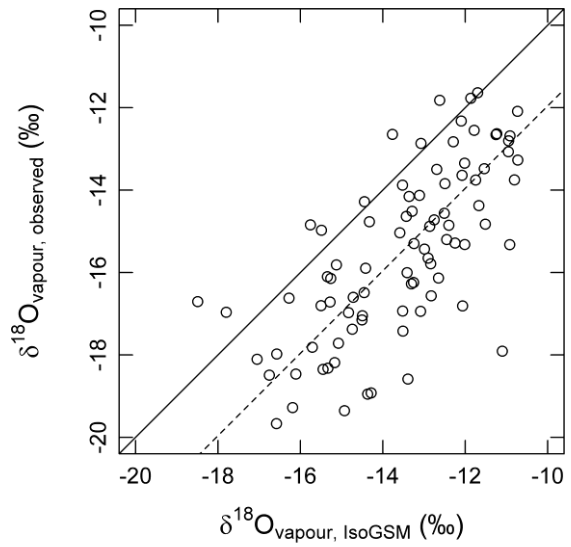

Figure S4: Relationship between the $\delta^{18}O$ of atmospheric water vapour as measured at the experimental site ($\delta^{18}O_{vapour,\ observed}$) and predicted by IsoGSM ($\delta^{18}O_{vapour,\ IsoGSM}$). The solid line represents the 1:1 relation; the dashed line gives the mean difference between the two data sets (–2‰).

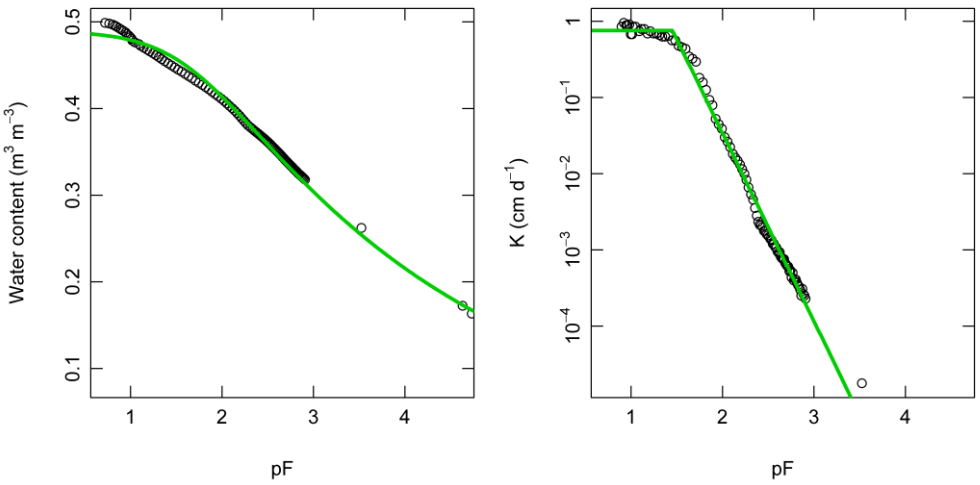

Figure S5: Relationship between volumetric water content (m^3 water m^{-3} soil) and pressure head, given as pF value (common logarithm of the pressure head in hPa), (left panel), and hydraulic conductivity (logarithmic scale) and pressure head (right panel), as derived from Hyprop measurements (open circles). The green curve in the left panel represents the Van Genuchten water retention curve fitted to the data, the green curve in the right panel shows the Brooks-Corey hydraulic conductivity curve fitted to the conductivity data. Derived parameter values are given in Table S1.

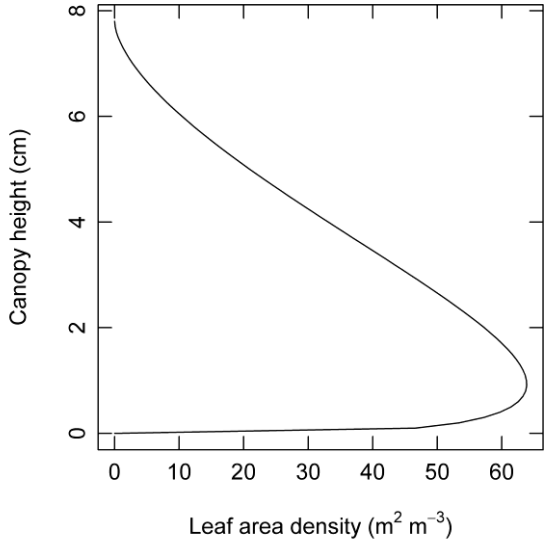

Figure S6: Beta distribution describing the assumed vertical leaf area density distribution at the experimental site (based on Wohlfahrt et al., 2003).

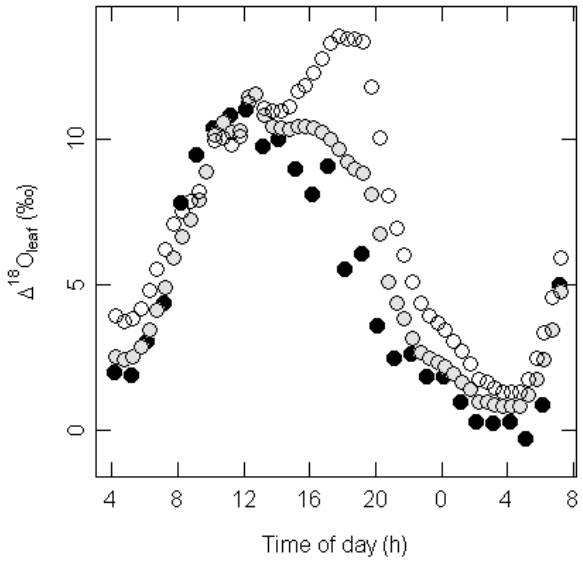

Figure S7: Diurnal time courses of ^{18}O-enrichment of leaf water ($\Delta^{18}O_{leaf}$) observed (closed circles) on 4/5 August 2005 in pasture paddock no.8 at Grünschwaige and predicted using the two-pool model with a constant proportion of unenriched water ($\varphi = 0.39$; grey circles) and the Péclet model with a constant effective length ($L = 0.162$ m; open circles). Predicted and observed $\Delta^{18}O$ was calculated as the difference between $\delta^{18}O$ of leaf water and $\delta^{18}O$ of soil water at 7 cm depth. Observed $\delta^{18}O_{soil}$ at 7 cm depth was obtained from linear interpolation between the $\delta^{18}O_{soil}$ at 2 cm and 12 cm depth. Time is given in UTC.

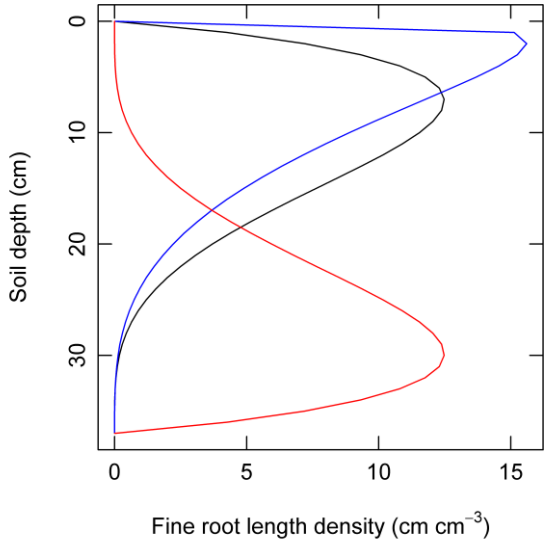

Figure S8: Beta distribution of fine root length density *versus* soil depth. The black line, with highest root density at 7 cm belowground, represents that used in the standard MuSICA runs; blue and red lines give the low and high alternative root distributions used in the sensitivity analysis (see Fig. 6h in main text), with maxima of root length density at 2 and 30 cm depth, respectively. All distributions have the same total fine root length (19 km m^{-2} soil surface).

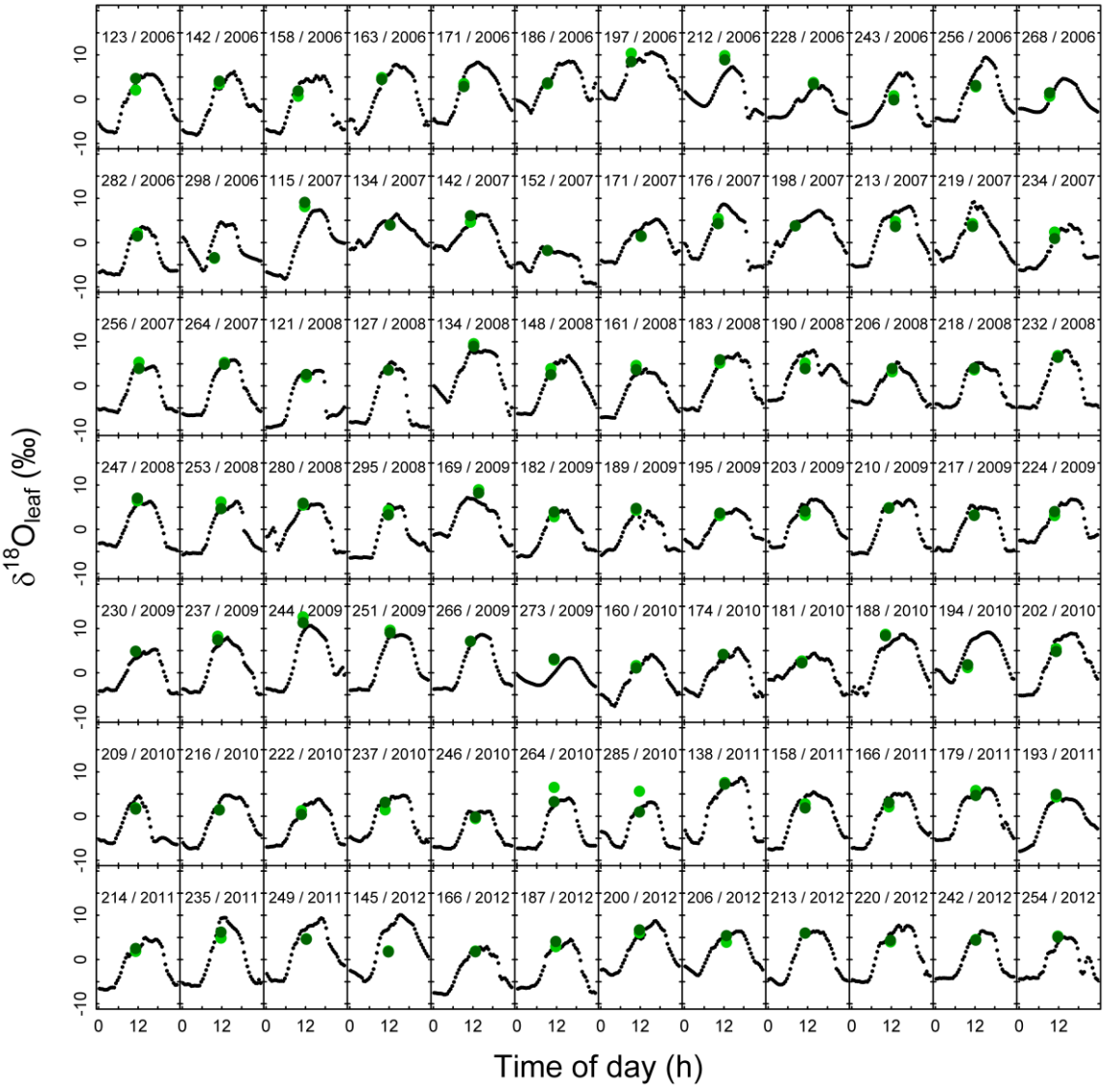

Figure S9: Diurnal cycles of modelled $\delta^{18}O$ of leaf water (black dots) and measured $\delta^{18}O$ of the two replicates of leaf water for all sampling dates (light and dark green dots). Numbers in the panels give the day of the year and year. Time is given in UTC.

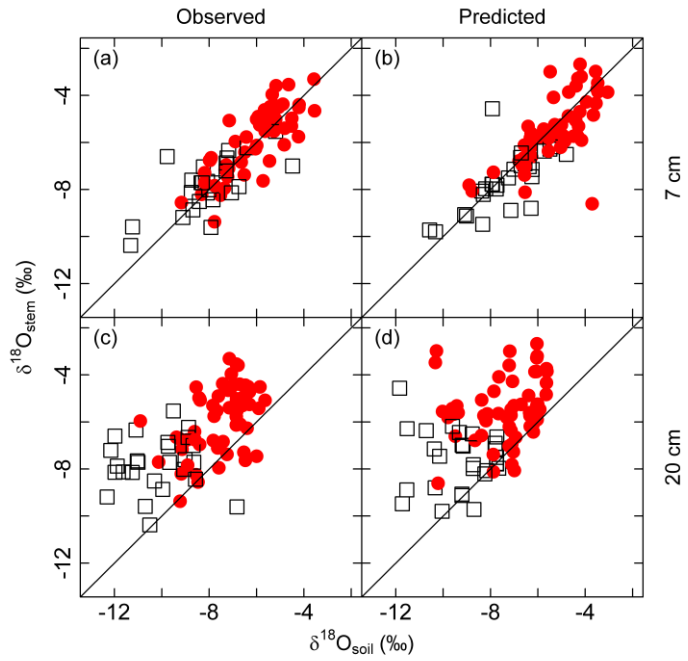

Figure S10 Correspondence between the $\delta^{18}O$ of stem water and soil water at 7 (upper panels) and 20 cm depth (lower) as observed (left) and predicted (right) in the first half (April to June; black squares) and in the second half of the vegetation period (July to October; red circles). The straight lines represent the 1:1 relationship.

5

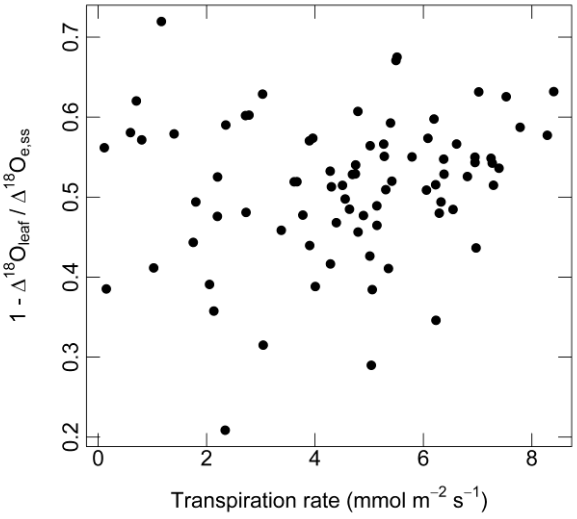

Figure S11: Relationship between canopy transpiration rate and the proportional difference between observed leaf water enrichment ($\Delta^{18}O_{leaf}$) and $\Delta^{18}O$ at the evaporative site, as predicted by the Craig-Gordon model ($\Delta^{18}O_{e,ss}$).

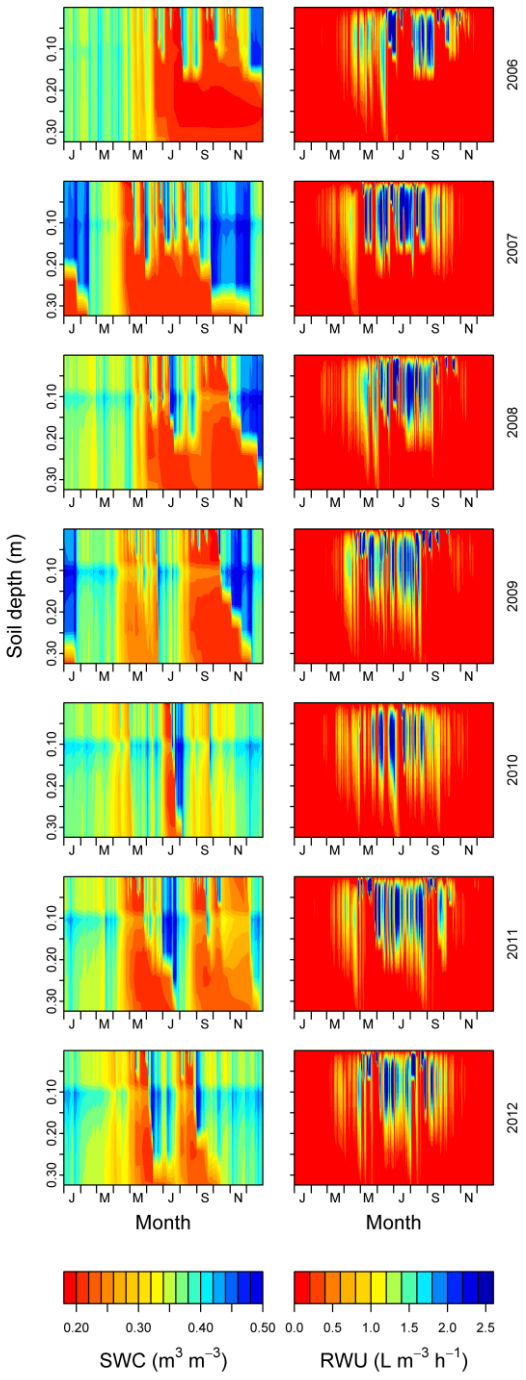

Figure S12: Soil water content (SWC) and root water uptake (RWU) along the soil profile as predicted by MuSICA for the studied period (2006-2012). The year is indicated on the right hand side.

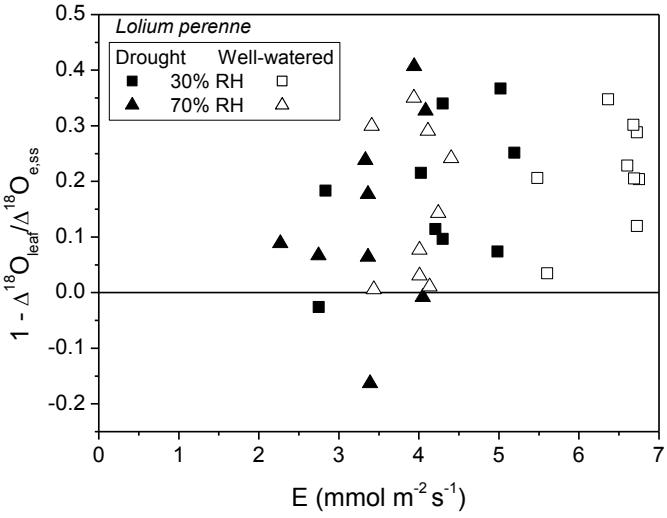

Figure S13: The relationship between transpiration rate (*E*) and the proportional difference between measured leaf water and the Craig-Gordon predicted enrichment ($1 - \Delta^{18}O_{leaf}/ \Delta^{18}O_{leaf}$) for *Lolium perenne*. The relationship in Fig. S13 is statistically significant, but very weak: $1 - \Delta^{18}O_{leaf}/ \Delta^{18}O_e = 0.017\ E + 0.035$; $r^2 = 0.11$; $P = 0.045$.

5

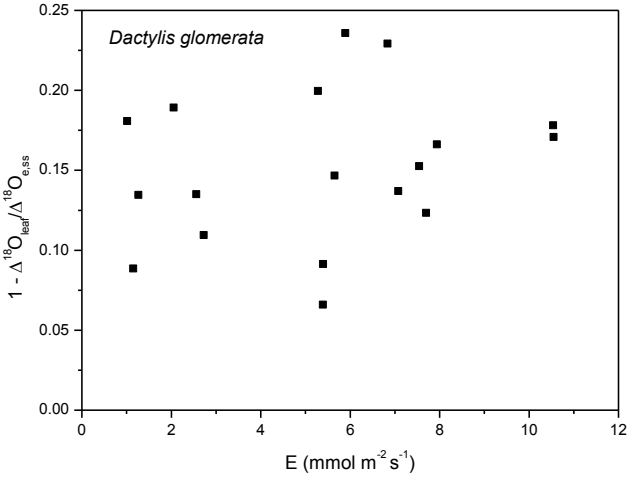

Figure S14: The relationship between transpiration rate (*E*) and the proportional difference between measured leaf water enrichment and that at the sites of evaporation ($1 - \Delta^{18}O_{leaf}/ \Delta^{18}O_e$) within the leaf for *Dactylis glomerata*.